Long term creep and stress rupture of aramid fibre

G. M. Fallatah, N. Dodds and A. G. Gibson

The present paper describes a creep rupture investigation on aramid fibre yarns (Twaron 1000 and Kevlar 29) supplied by Teijin and Du Pont respectively. The ISO 9080 extrapolation procedure, which was developed for thermoplastic pipe materials, was used to model and interpret the results. The 4 parameter version of this procedure fitted the results well and gave useful predictions of the long term stress rupture behaviour, lending confidence to existing qualification procedures for the use of aramid fibre in reinforced thermoplastic pipe (RTP), and other applications involving continuous high tensile loads. Creep strain measurements on yarns showed a near constant degree of creep deformation per decade. Although they may involve some of the same mechanisms the creep and stress rupture processes appear to operate independently and on different time scales. It was found that creep deformation in aramid yarns is unlikely to be a significant problem at stress levels corresponding to a 20 year lifetime.

Keywords: Aramid, Creep, Stress rupture

Introduction

Aramid is the most successful member of a range of ultrahigh strength polymer fibres developed over the last forty years. Frank[1] in 1970 discussed routes by which high strength and stiffness might be achieved in polymers by making use of the fully chain extended conformation, where the intrinsic properties of the carbon–carbon covalent bond could be exploited. Successful research in the 1970s (Ref. 2) resulted in the manufacture of high strength polymers by virtually all of the routes proposed in that paper, including polyethylene fibres manufactured by ultradrawing and gel spinning. Rigid rod polymers, however, which have been widely studies in the last three decades[3–14] provide stability up to higher temperatures than extended chain thermoplastics, but are much more challenging to process because of their intractability to melt processing. Use must be made instead of their solubility in highly polar media, in which they show lyotropic liquid crystal behaviour. This phenomenon, and the effects of orienting flows, enable aramids to be processed by wet spinning into fibres with a high level of crystallinity and molecular orientation. The molecular structure of para-aramid[2,4,12,13] is shown in Fig. 1.

Aramid fibre successfully penetrated a wide range of markets, including tyres, tension members, composite products and ballistic protection fabrics. However, an important new market that has emerged in the last 15 years is reinforced thermoplastic pipe (RTP).[15] This fulfils of the need of the oil and gas industry for flexible high pressure pipework with greatly improved resistance to oilfield fluids, especially those containing dissolved H_2S and CO_2 which are highly corrosive to steel. While unreinforced thermoplastic pipe can only offer working pressures up to ~15 bar, RTP is capable of offering working pressures of 80 bar and much higher. An advantage of aramid in this application is that, unlike glass and carbon fibre, aramid does not need to be fully impregnated with and protected by resin in order to work effectively. This is because, along with its sizing system, aramid provides yarns with a low friction coefficient that are much more resistant to damage by fibre–fibre abrasion than the other fibres.

Reinforced thermoplastic pipe, as shown in Fig. 2, comprises a thermoplastic liner and cover, reinforced by an even number of aramid fibre reinforcing layers, wrapped at $\pm 55°$ to the pipe axis, the optimum angle to resist internal hydrostatic pressure. The product is manufactured in diameters up to 6" (150 mm), with working pressures, depending on the application, up to 12 MPa (120 bar). There are currently two manufacturers, Pipelife bv and Technip. The first applications were in onshore transport of oilfield fluids, as shown in Fig. 3, as well as in gas transmission. Despite being significantly more expensive than steel, RTP has the advantages of corrosion resistance and flexibility, which provides ease of deployment, as shown in Fig. 4. More recently, subsea applications have arisen, as shown in Fig. 5.

The possible use of large volumes in RTP represents a technical challenge for aramid because this is one of the fibre's most highly continuously stressed applications. This has generated renewed interest in its long term creep rupture behaviour. To promote the wider

Centre for Composite Materials Engineering, School of Mechanical & Systems Engineering, University of Newcastle upon Tyne, Newcastle upon Tyne NE1 7RU, UK

*Corresponding author, email a.g.gibson@ncl.ac.uk
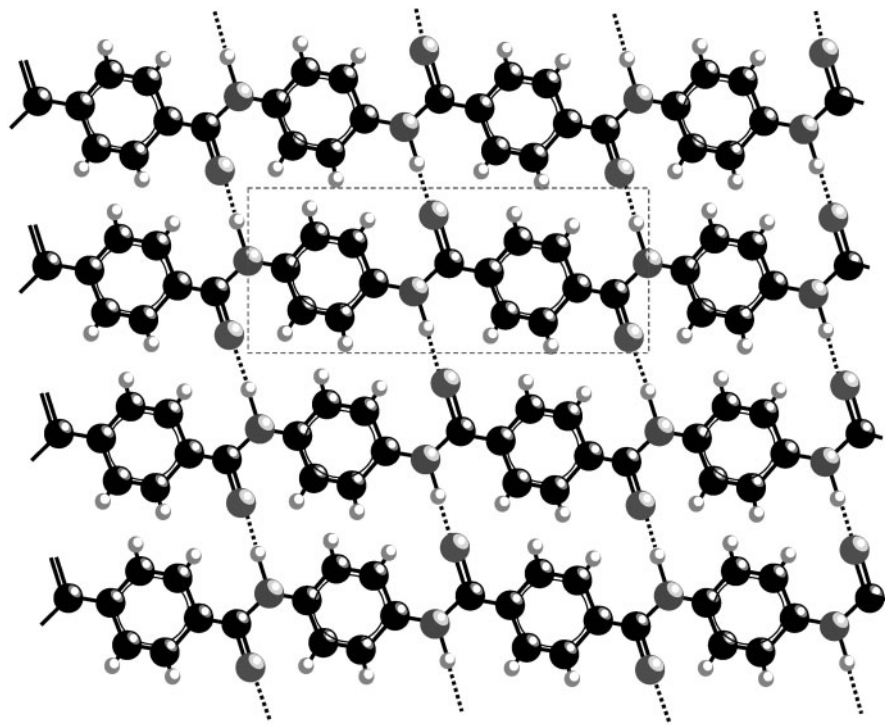
1 Crystalline structure of aramid fibre, showing *b–c* plane: unit cell dimensions[9–14] are *c* (chain direction)=1·29 nm and *b* (transverse direction)=0·518 nm, *a* direction dimension, not shown, is 0·787 nm
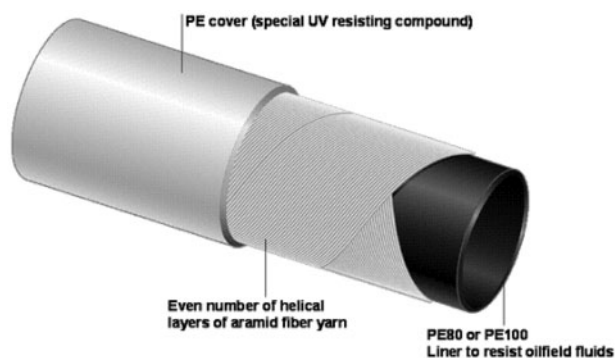
2 Schematic structure of RTP, showing liner, reinforcement and cover (Courtesy of Technip)

application of RTP, the principal manufacturers, together with Teijin, Du Pont and a group of end users formed a joint industry project (JIP), which was recently successfully completed.[16,17] The JIP outputs comprised guidelines for the qualification and use of product,[16] including an API Guideline[18] for oilfield applications and an ISO Technical Specification for its use in gas transmission.[19]

Qualification of reinforced thermoplastic pipe

All non-metallic pipe systems are prone to long term failure under load, through processes involving creep

3 Aramid fibre RTP in use for transport of oilfield fluids: photograph shows white pigmented, UV stabilised cover for exposed use in hot climates, as well as electrofusion coupler technology, which is one of jointing options (Courtesy Pipelife bv)

4 Flexibility of RTP permits coiling on drum: continuous lengths, up to 1 km between joints, may be deployed (or retrieved) by this simple means (Courtesy of Technip and Petroleum Directorate Oman)
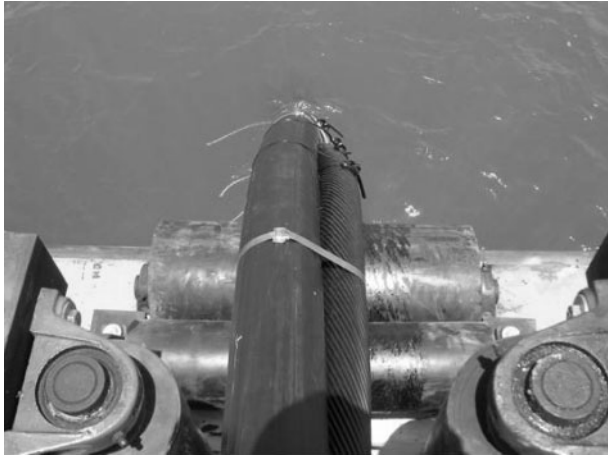
5 Piggyback deployment of underwater RTP, alongside steel cable (Courtesy of Technip)

and/or damage accumulation, the process generally referred to as stress rupture or static fatigue. The main financial burden in the qualification of non-metallic piping products is the cost of this long term stress rupture testing, which involves the application of constant pressure and the measurement of failure times exceeding 10 000 h, as shown schematically in Fig. 6. This enables a relationship to be established between the applied pressure and the time to failure. A statistical lower prediction limit (LPL) is then calculated for the product, as shown, and extrapolated to the design life, to enable a long term pressure rating to be established for the pipe. Using the LPL, rather than the mean line enables some allowance to be made for the variability of the product, as manufactured. Most non-metallic pipe systems, including thermoplastic and fibreglass pipe, employ similar procedures.[20,21]

The JIP investigated a number of ways in which the burden of long term testing might be reduced. A key task was to characterise the long term failure behaviour of aramid yarns, representative of the reinforcement used in RTP. The outcome of this task is reported here,

along with an interpretation of aramid fibre creep behaviour.

Theory for qualification tests

Reinforced thermoplastic pipe qualification tests assume an empirical power law relationship between time to failure and pressure (at constant temperature). In other words, a linear relationship is assumed between these quantities when plotted on a log–log basis, as in Fig. 6. This form of relationship is assumed in almost all types of non-metallic pipe qualification procedures, including Refs. 18–21. Since, for RTP, fibre failure is the key failure mechanism, the aramid yarns are also assumed to behave in the same way, so the following relationship was assumed between the applied stress σ and the time to failure t_f

$$\sigma = F t_f^{-G} \tag{1}$$

so the equation of the stress rupture curve is

$$\log \sigma = \log F - G \log t_f \tag{2}$$

where F and G are power law constants, $-G$ being the regression line slope.

Alternatively, in terms of time to failure

$$t_f = \left(\frac{F}{\sigma}\right) \frac{1}{G} \tag{3}$$

In the case of RTP[16,18,19] the regression relationship for the stress rupture behaviour is determined at the 'design temperature', the maximum temperature at which the product will be used and failure points are required up to times exceeding 10 000 h, somewhat more than one year. The LPL for the results is the lower 95% confidence limit for individual experimental points. This represents the line above which 97·5% of all individual measurement points should lie. The design basis and pressure rating of the pipe is then determined by extrapolating the LPL to the design life, which in the case of most oilfield pipework, is 20 years. This value is the manufacturer's nominal pressure rating (MNPR). It
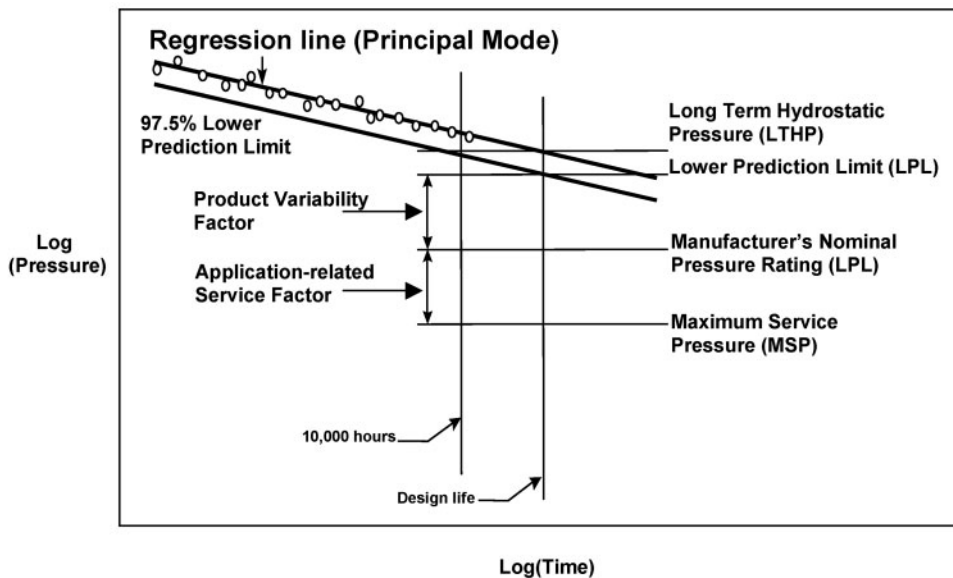
6 Schematic of pressure rupture relationship for reinforced thermoplastic pipe, showing experimental results, mean line and extrapolation of the LPL to design life
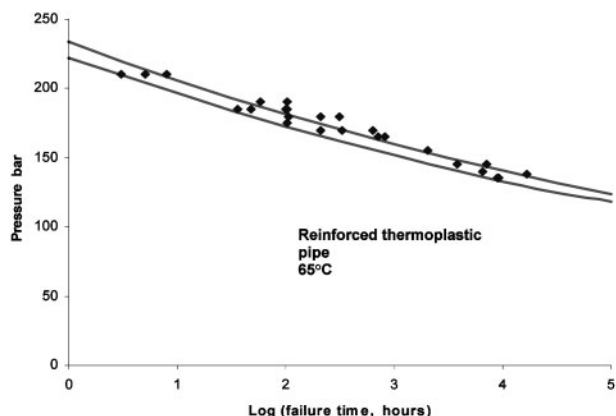
7 Pressure versus log time to failure relationship for Pipelife RTP at 65°C (Courtesy, Pipelife bv)

is regarded as reasonable practice to extrapolate such failure data by up to ~1·5 decades. Generally, depending on the individual application and the fluid being handled, a further safety factor will be applied to the MNPR to determine the working pressure, but the MNPR is the key factor determining the rating of the pipe. Extrapolating the LPL, rather than the mean line takes into account the manufacturing variability of the product, which is assumed to be the main factor determining the scatter on the failure points.

Figure 7 shows an example of one manufacturer's regression data, along with the mean line and the LPL, for a particular RTP product. In this case the scatter on the data is fairly small, so the LPL is quite close to the mean line.

Temperature dependence

The ISO 9080 procedure[21] requires measurements to be taken at different temperatures. If Arrhenius dependence is assumed for the time to failure, equation (3) can be amended to

$$t_f = A \exp\left(\frac{H}{kT}\right)\sigma^{-\frac{1}{G}} \tag{4}$$

where H is the activation energy of the process and k is Boltzmann's constant.

This model makes no assumptions about the physical mechanisms involved in the creep and failure of the fibres. The alternative approach would be the widely used model due to Eyring,[22] which assumes creep deformation to consist of a series of thermally activated events. In this case the failure time would be

$$t_f = A \exp\left(\frac{H-V\sigma}{kT}\right) \tag{5}$$

where the constant V is the activation volume.

Eyring has been employed with some success to model the creep and failure of aramid fibre.[6,7,12] The model predicts a linear relationship between stress and log time to failure, instead of the power law relationship of equation (1).

The plastic pipes industry has considerable experience of modelling the stress rupture of pipe materials at long times, over a range of temperatures. Standards and qualification procedures invariably use the power law model rather than Eyring, although in most cases each would fit the results equally well. The reason for

preferring the power law model is simple: extrapolation of failure data assumed to be linear in log–log space gives a slightly more favourable life prediction than the equivalent extrapolation in lin–log space.

ISO 9080[21] contains a useful modelling and extrapolation protocol for modelling failure data. The same approach has been recommended for modelling other types of failure data. ISO 9080 assumes that the time to failure is given by an expression of the form

$$\log(t_f) = c_1 + \frac{c_2}{T} + c_3\log(\sigma) + \frac{c_4\log(\sigma)}{T} \tag{6}$$

where c_1, c_2, c_3 and c_4 are fitting constants, and T is the absolute temperature. Comparing this with equation (4) it can be seen that the constants are related by

$$\log A = c_1 \tag{7}$$

$$H = 2{\cdot}302585kc_2 \tag{8}$$

$$G = -\frac{1}{c_3 + \frac{c_4}{T}} \tag{9}$$

Finally

$$\log F = \frac{-c_1 - \frac{c_2}{T}}{c_3 + \frac{c_4}{T}} \tag{10}$$

In terms of temperature dependence the rupture curves are taken to be proportionally spaced depending on the reciprocal of the absolute temperature. This is consistent with creep and failure being governed by an Arrhenius type thermally activated process, as implied in equation (4). The regression procedure obtains the best least squares fit for the constants based on the scatter in $\log t_f$, i.e. on the scatter in the 'ordinate' direction. This has been shown to be more conservative than using the vertical scatter (i.e. the scatter in $\log\sigma$). Two versions of the protocol are available: the three parameter model ($c_4 = 0$) where all the regression lines have the same slope in log–log space, and the 4 parameter model ($c_4 \neq 0$) where the slope varies with temperature.

Calculation procedures for the least squares fit and the LPL are explained in ISO 9080[21] and will not therefore be discussed here. In addition to curve fitting and extrapolation, the standard also provides methods for checking possible changes of slope due to changes in failure mode of the material. Such a change, which would be indicated by a 'knee' in the curve, would indicate undesirable long term performance. Including test data at temperatures higher than the intended design temperature is very important in this respect, because undesirable failure mechanisms tend to move to shorter times as the test temperature is increased.

Experimental

Creep rupture tests at constant load were carried out on aramid fibre yarn in air at 25, 65, 95 and 120°C. At 25 and 60°C, failure times exceeding 10 000 h were achieved. For the other temperatures, failure times were limited to ~1000 h.

The principal aim was to establish values of the regression line gradient and 20 year design parameters for the fibre yarns, especially at the most frequently used design temperature of 65°C. A secondary aim was to look for any evidence of any long term changes in failure
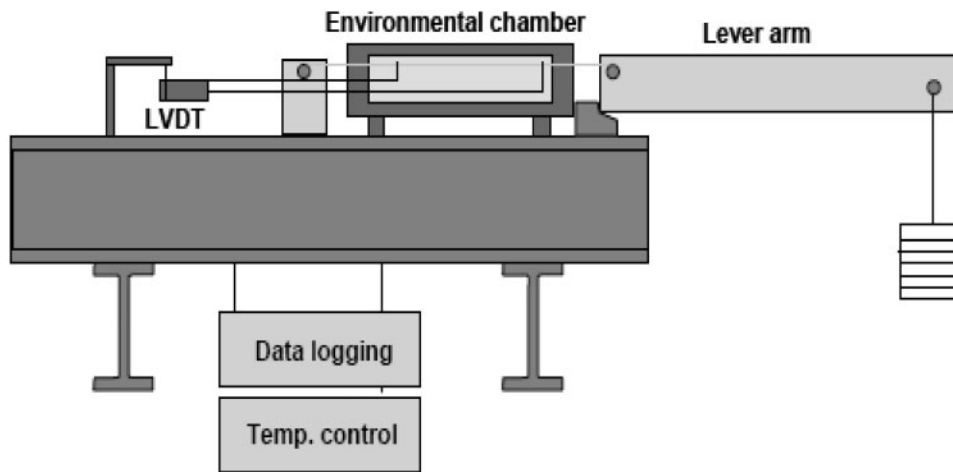
8 Schematic of dead loading stress rupture testing machine

mode that would affect the suitability of the fibre for long term use.

The two yarn types in the study were Kevlar 29 (1670 dtex) and Twaron 1000 (1680 dtex). Although the manufacturing processes employed by Teijin and Du Pont differ in certain details these yarn products are acknowledged to be very similar in performance and have been regarded as effectively interchangeable. It is worth pointing out that Kevlar 29 differs from Kevlar 49, the fibre type most widely used in composite materials and the material for which most long term performance data arecurrently available. Kevlar 49 is subjected to a more prolonged stretching treatment to improve orientation, as a result of which it possesses a higher Young's modulus than Kevlar 29, but similar strength.

Behaviour of yarns is influenced by the level of twist. There is a statistical variation of strength along each fibre, due to a distribution of flaws or weak points in the constituting filaments of the fibre (in this case 1000 filaments). With untwisted fibres, therefore, test results depend on the gauge length, and a Weibull analysis of the results would be required. Twisted yarns largely eliminate this variation by allowing stress to be shared, through friction, between adjacent filaments when a particular filament fails. This is similar to the 'composite' effect achieved when fibres are impregnated by a rigid resin matrix. Both yarns were supplied with the same twist level of 'z80' (i80 turns per metre), which was representative of the yarns currently employed to reinforce RTP.

Stress rupture tests were carried out using seven temperature controlled dead loading rigs, designed for testing aramid fibre, as in Fig. 8. In addition a computer controlled mechanical testing machine, equipped with a temperature controlled oven, was used in constant load mode for a number of the short term tests, lasting up to ~100 h. In all cases, cylindrical grips of the capstan type were employed, to minimise grip damage to the yarn and grip failure. There were a small number of results involving grip failure and these were discarded.

Once sufficient data were available to determine the approximate shape of the regression relationships for the yarns, some further experiments to measure creep strain were put in place. The strain within a 100 mm gauge length was measured using a linear voltage differential transformer (LVDT) transducer, in the arrangement shown in Fig. 8. These measurements were carried out

at just two temperatures, 25 and 65°C. The LVDT was held on a compliant suspension, which allowed frictionless lateral movement. The LVDT body and core were connected to respective ends of the gauge length by lightweight carbon fibre rods and steel pins. The pins were carefully inserted between the fibres in the yarn, to avoid fibre damage and, with the yarn under a small pretension, anchored in position with a very small bead of cyanoacrylate adhesive. This arrangement was found to work well for the most part. Some difficulties were found in establishing a reproducible level of initial elastic strain after the first application of the load. These were largely overcome by applying and removing small loads until the strain zero position could be accurately and reproducibly established. The other experimental difficulty, which was not overcome, was the problem of accurately measuring the very small residual creep rate that occurred at lower loads, when measurement times exceeded 1000 h. For this reason and for reasons of available time the period of measured creep strain seldom exceeded 1000 h.

Results

Figures 9 and 10 show the stress rupture results on the two different yarns in air. The slopes of the curves varied with temperature, so the 4 parameter model was required. The procedure was effective in correlating the behaviour at different times and temperatures. The regression constants and the 20 year LPL values were calculated and are given in Table 1. It can be seen, from comparison with Fig. 7, that the scatter of the failure

Table 1 Regression results for aramid fibre yarns: ISO 9080 prediction parameters*

	25°C		65°C	
	G	*F*	*G*	*F*
Kevlar	0·03682	2·2085	0·04919	2·0958
Twaron	0·04237	2·2278	0·05402	2·1961
	95°C		120°C	
	G	*F*	*G*	*F*
Kevlar	0·06179	1·9867	0·07569	1·8730
Twaron	0·06485	2·1228	0·07573	2·0518

*Numerical values of *F* correspond to stresses in GPa and failure times in hours. Values accurate to 2–3 significant figures, but further figures are given to assure similarity of calculations.
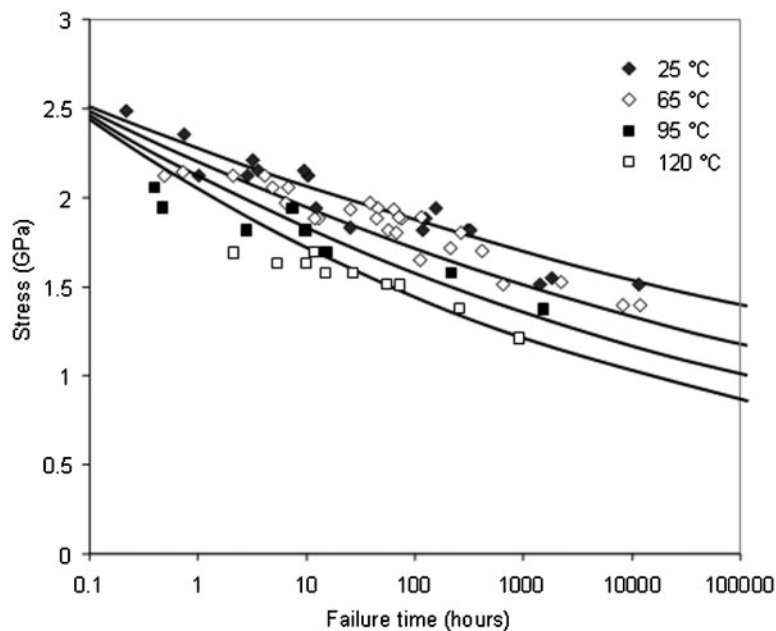
9 Twaron 1000 yarn results: continuous lines are predictions of ISO 9080 4 parameter model

points for the yarns in tension is significantly greater than that observed when testing RTP spool samples under pressure. In hindsight it was realised that this was because, when a pipe was tested, the behaviour of several hundred yarns was effectively averaged, which greatly reduced the scatter. Despite the scatter problem, however, the actual failure parameters are rather similar for the two different yarn types, confirming that the products are effectively interchangeable.

The values of the regression line slope *G* are close to the values measured on pipes and used by RTP manufacturers in rating their products. This is interesting, as it had been anticipated that the regression line slopes for the yarns themselves might be a little shallower than those for pipe samples. The implication is that the manufacturing processes used to convert the yarns into reinforcing tapes and to incorporate the tapes into the RTP must be very effective in achieving an even distribution of strain between all the yarns. The view of the RTP JIP was that one of the consequences of strain imbalances between yarns would be an increase in the regression line slope. The similarity seen here between the yarn data and pipe data supports the idea that these products were well manufactured, from the viewpoint of strain balance, and the pressure regression test is therefore a good test of RTP quality. It may be that future qualification procedures could avoid the 10 000 h regression test sequence, replacing it with a test for conformity of the regression line slope.

Applying the test criteria of ISO 9080, there is no evidence at all of any 'knee' in the curves, either at long times or higher temperatures. This was checked both visually and using the mathematical procedure provided
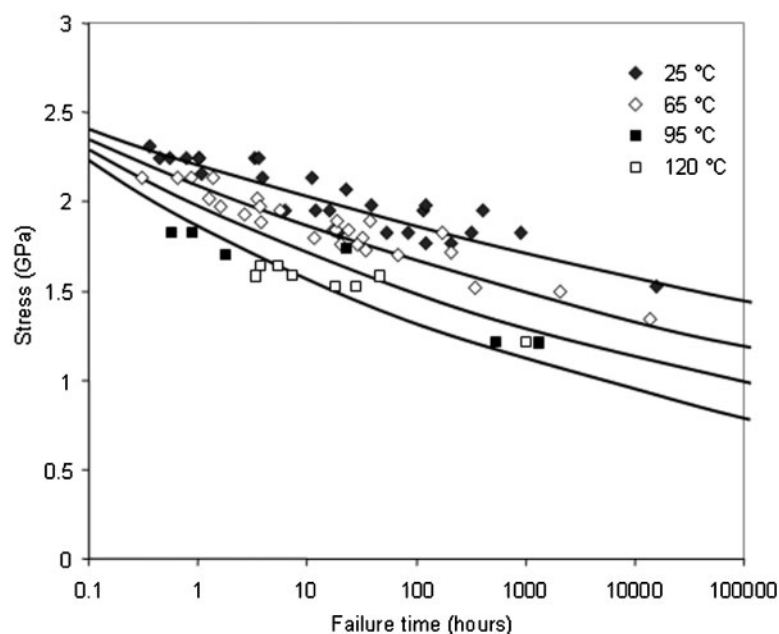
10 Kevlar 29 yarn results: continuous lines are predictions of ISO 9080 4 parameter model
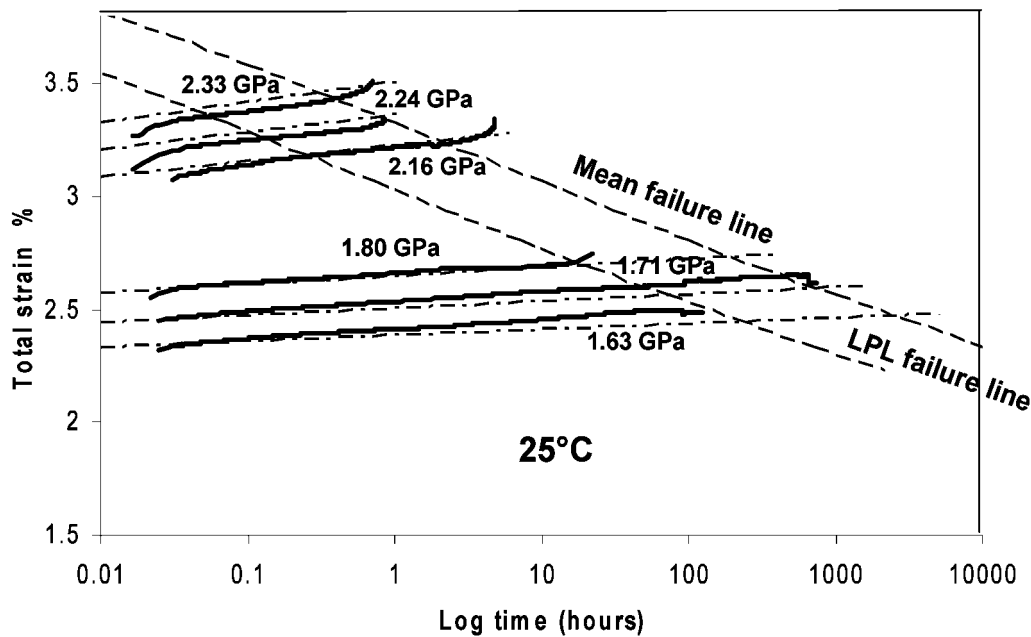
11 Creep behaviour for aramid yarn at 25°C, at stresses of 2·33, 2·24, 2·16, 1·8, 1·71 and 1·63 GPa: continuous lines are experimental data: predictions of equation (12) are shown, along with mean and LPL failure lines

in the standard. This useful result suggests that there will be no change of failure mechanism at long times at the maximum design temperature of 65°C, giving confidence in the use of aramid reinforcement.

The ISO 9080 procedure was rewritten, to incorporate the Eyring[22] rather than the power law model. It was found that the fit to the data was very similar to that observed in Figs. 9 and 10 for the power law model. For comparison purposes the 20 year mean failure stresses and 20 year LPL stresses are shown in Table 2. It can be seen that, as mentioned previously, the extrapolated values are slightly more favourable in the power law case, which appears to be the main justification for using this procedure.

Table 2 Comparisons between 20 year mean failure stress and 20 year LPL from power law (log–log) and Eyring (lin–log) models, using mathematical procedure of ISO 9080

Power law (log–log)		
Kevlar, °C	Mean, GPa	LPL, GPa
25	1·416	1·283
65	1·157	1·018
95	0·942	0·774
120	0·751	0·521
Twaron, °C	Mean, GPa	LPL, GPa
25	1·365	1·226
65	1·144	1·001
95	0·970	0·801
120	0·822	0·600
Eyring (lin–log)		
Kevlar, °C	Mean, GPa	LPL, GPa
25	1·328	1·135
65	1·016	0·790
95	0·762	0·453
120	0·534	0·073
Twaron, °C	Mean, GPa	LPL, GPa
25	1·277	1·068
65	0·995	0·757
95	0·773	0·456
120	0·580	0·125

Values accurate to 2–3 significant figures, but further figures are given to assure similarity of calculations.

Figures 11 and 12 show the measured creep strains at 25 and 65°C respectively. The general features, as reported previously[5,6,14,22] for Kevlar 49, are a rapid, mainly elastic response, followed by a low rate of creep deformation. It does appear that a short relaxation process may take place in the first minutes after loading, as it takes some minutes for the curves to level out. After this, the creep rate, per decade appears to be almost constant, as has been noted before.[5] A constant creep rate in linear time, which is observed with many materials in the secondary stage of creep, would imply an upwardly curving creep response in logarithmic time, which does not appear to occur in the present case. This, of course, implies the existence of some 'hardening' process, as the creep rate is, in effect slowing down with time. The creep rate per decade appears to be a strong function of stress, as it reduces to a very low rate for stresses that would cause failure at times of 10 h and beyond.

It seems probable, observing the differences in time-scale between the stress rupture data and the creep data, that mechanisms involved in the two different processes may be different.

Discussion

Structure and properties of aramid fibre

The structure and properties of aramid fibre have been widely investigated.[2–14,23] Unlike thermoplastic fibres, aramid has a structure that is close to 100% crystalline. Poly *p*-terephthalamide (PPTA) possesses a monoclinic unit cell, with the chains linked in the *b* direction by regular hydrogen bonds, as shown in Fig. 1. The *b–c* plane dimensions have been established as $c=1\cdot29$ nm and $b=0\cdot518$ nm,[13] the phenyl units being arranged so that they lie almost in the same plane. The intractability of aramid to melt processing derives principally from the rigidity of the chain direction bonds and the chain length, which may exceed 5000 repeat units. The inter-chain hydrogen bonds contribute to this intractability
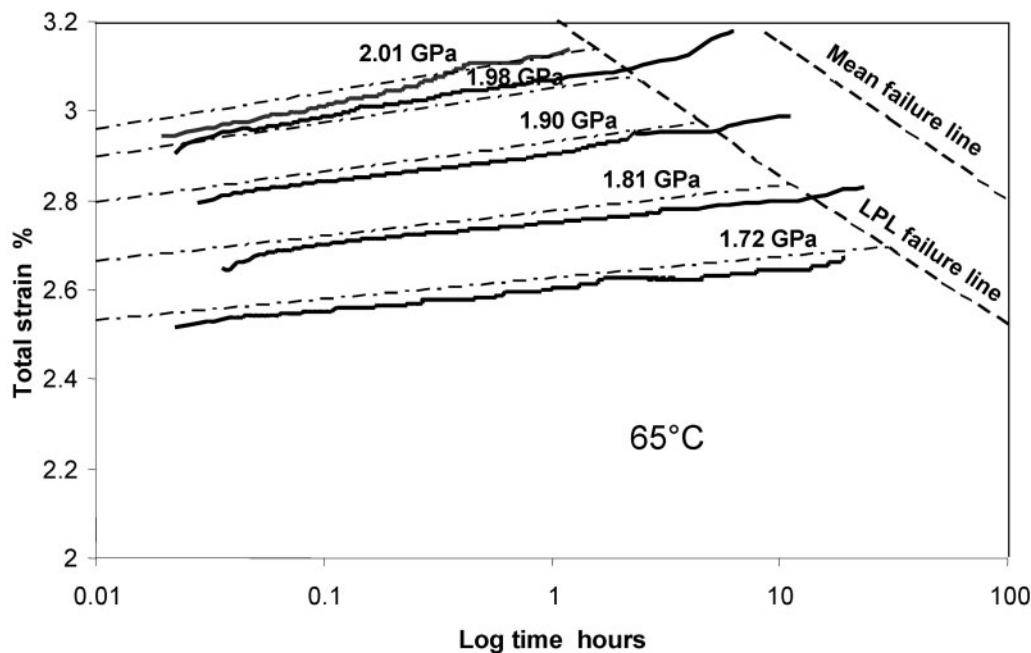
12 Creep behaviour for aramid yarn at 65°C, at stresses of 2·01, 1·98, 1·97, 1·9, 1·81 and 1·72 GPa: continuous lines are experimental data; predictions of equation (12) are shown, along with mean and LPL failure lines

and promote a crystalline phase with a two-dimensional lamellar structure, there being relatively weak bonding in the *a* direction. There is less certainty about the *a* direction dimensions, stated to range from 0·435 to 0·56 nm and about the orientation of the *b–c* layers relative to one another through the crystal thickness.[9–11,13,14,23] The weak *a* direction interactions provide the possibility of variations in the structure in this direction, due to stacking faults, etc.

Rigid rod polymers contain various types of crystalline imperfection but there are no chain folds of the type found in semicrystalline plastics and no identifiable amorphous phase. Therefore the conventional causes of viscoelasticity are largely absent. The rigid crystalline sequences extend for virtually their full length within the crystallites – one of the factors that accounts for the high strength and stiffness of aramid fibre. The weak *a* direction bonding, in addition to the well known pleated structure of the crystalline phase, which occurs on a larger scale, accounts for the relatively low value of the compressive strength of aramid. The weak *a* direction bonding also probably accounts for the low friction coefficient and, paradoxically, the resistance to damage through fibre–fibre interactions.

Important features of the tensile creep behaviour of para-aramid are that a high tensile load produces an elastic response followed by a small, long term creep process which continues up to the point where the fibre fails. The long term creep strain is only partially recoverable, indicating that at least one mechanism of plastic deformation is present.

The most probable deformation mechanism in aramid fibre, bearing in mind the crystalline structure (Fig. 1), is slip on the *b–c* plane. *a–c* slip may also be possible, but this would involve breakage and possibly the reforming of the interchain hydrogen bonds. The most notable work on the tensile creep behaviour of aramid fibre was carried out by Northolt and co-workers,[14,23] who proposed that the principal plastic deformation mechanism comprises chain direction shear of the crystalline phase in regions of imperfect fibre orientation. This is the most widely accepted model for aramid. Although there are some small difficulties associated with the fact that the molecular orientation is quite high, with orientation functions close to unity, the theory otherwise accounts successfully for most of the observed phenomena, including the fact stress–strain curves in these materials showing a slight, but significant upward curvature,[5,14,23] presumably due to this improvement in orientation. Northolt *et al.*[14,23] mention that it is generally unnecessary to take account of the fact that the chain shear process will result in an improvement in orientation function as the crystalline domains rotate to an orientation nearer to the deformation axis, which, again, is a reasonable assumption.

It seems probable that the mechanisms of stress rupture and of creep are similar in that they involve slip processes of the type discussed here. However, these processes appear to take place with different stress dependence over different timescales. It seems probable that stress rupture involves the growth of flaws either from preexisting voids within the material or as a result of deformation processes near to the ends of low molecular weight crystalline sequences in the material. It is also probable that this process involves only a very small proportion of the material. This is supported by the observation that there is no evidence of a reduction in Young's modulus of the fibre during this damage growth process. Indeed there are some indications of a small increase in Young's modulus, as observed by others, due presumably to an improvement in crystalline orientation. If there were bulk changes in the distribution of stress between crystalline sequences this would undoubtedly show up as a change in modulus.

The increase in creep strain, by contrast seems to involve all of the material. It may result from widely distributed changes in the stress distribution around the ends of crystalline sequences and from small movement
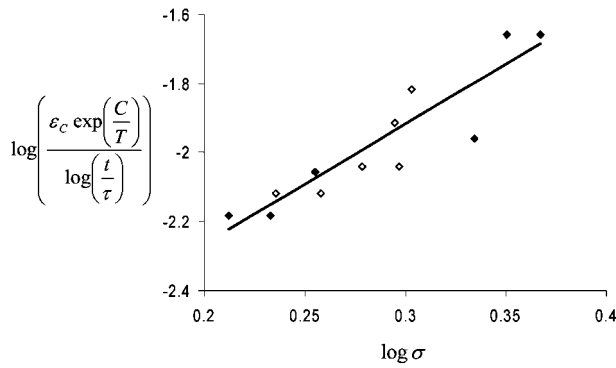
13 Plot of $\log\left[\varepsilon_C \exp\left(\frac{C}{T}\right)/\log\left(\frac{t}{\tau}\right)\right]$ versus $\log\sigma$ for creep results at 25°C (closed symbols) and 65°C (open symbols)

14 Creep prediction for aramid yarn at 65°C, for different stress values: mean and LPL failure lines are also shown

of these sequences relative to one another. Unlike the mechanism involved in stress rupture, it does not appear to be damaging overall to the material.

Creep model

The creep data in Figs. 11 and 12, for 25 and 65°C, suggest that the creep strain at high stresses increases linearly with logarithmic time. This implies that the creep rate actually declines with increasing time, suggesting a hardening mechanism. If the creep component is governed by an Arrhenius process and is related in a power law manner to stress, it might be expected that the creep component of strain ε_C would be given by

$$\varepsilon_C = A \exp\left(\frac{-C}{T}\right) \sigma^n \log\left(\frac{t}{\tau}\right) \qquad (11)$$

where A, C and n are constants. The factor τ is necessary to provide a datum for the logarithmic data. Taking $\tau = 0.01$ h effectively assumes that the decades of logarithmic time are measured from a starting point of 0.01 h. The strain at a particular time consists of both elastic and creep components, so the overall strain is

$$\varepsilon = \varepsilon_E + \varepsilon_C = \frac{\sigma}{E} + A \exp\left(\frac{-C}{T}\right) \sigma^n \log\left(\frac{t}{\tau}\right) \qquad (12)$$

where ε_E is the elastic component of strain and E is the Young's modulus.

The constants governing the creep component can be found from the creep data by rearranging equation (11) and taking logs, so

$$\log\left[\frac{\varepsilon_C \exp\left(\frac{C}{T}\right)}{\log\left(\frac{t}{\tau}\right)}\right] = \log A + n \log \sigma \qquad (13)$$

Figure 13 shows a plot of

$$\log\left[\varepsilon_C \exp\left(\frac{C}{T}\right)/\log\left(\frac{t}{\tau}\right)\right]$$

against $\log\sigma$ for the 25 and 65°C creep results. The constant C varied to minimise the mean squared scatter on this relationship, the optimum value being found to be 920 K. The constants A and n were found to be 1.093×10^{-3} and 3.48 respectively. It may be that, as was the case with the failure data, n varies somewhat with temperature. However, the variation in n from 25 and 65°C appears quite small and, given that creep data were only measured at two fairly close temperatures, n will be treated as constant in the present study. The

values of Young's modulus needed for the elastic term in equation (12) were 70 and 65 GPa respectively at 25 and 65°C. The choice of these values effectively determines the elastic baseline for the creep curves so the values chosen already take account of the relaxation that appears to take place immediately after loading.

By using the parameters determined from Fig. 14, equation (12) was used to estimate the creep behaviour at the temperatures and loads studied. The dotted lines in Figs. 11 and 12 are the predictions. Given the scatter on the creep data, these predictions agree quite well with the observed results. Of course the predicted creep strain values have no meaning beyond the point at which failure takes place, so 'failure' curves were added to Figs. 11 and 12. These were obtained by eliminating σ between the creep rupture relationship (equation (1)) and the creep model (equation (12)). The LPL line was calculated in a similar manner, solving the LPL relationship simultaneously with equation (1). It is interesting to note the significant decrease in strain at failure that occurs with increasing failure time. It is also interesting that, although the governing relationships are not linear, the failure limit curves are almost linear in strain versus log time.

Finally, equation (12) was used to predict the behaviour of aramid yarn at the long times typical of the design life of RTP. The results for 65°C are shown in Fig. 14. It is clear that, if the model applies at long times, creep deformation of aramid should not be a significant problem at any stress value below the level required to cause failure within 20 years.

Conclusions

Creep rupture measurements have successfully characterised the long term failure behaviour of aramid fibre yarns and provided data that can be used as the basis for future design in tensile applications, including RTP. Different yarn types showed very similar regression parameters.

Although the data scatter on individual yarn failure is larger than that for RTP spool samples the ISO 9080 4 parameter model provided a good description of stress rupture as a function of both time and temperature. The results suggest that there is unlikely to be a change in failure mechanism at long times, which lends confidence to the use of aramid fibre in highly loaded long term tensile applications.

The yarn regression lines showed an increase in slope with increasing temperature, the slopes being comparable to the slopes measured for RTP samples held under pressure at the same temperatures. Although the standard log–log form of the pressure versus time to failure relationship gave more optimistic predictions of long term behaviour than the lin–log form, based on the Eyring model, both models fitted the data equally well.

Measurements of creep strain showed that, over most of timescale investigated, the creep strain per decade is roughly constant, implying some structural change that reduces the rate of creep. The processes controlling the creep behaviour and the stress rupture behaviour appear to be independent of one another. The behaviour observed here implies that creep deformation of aramid fibre is unlikely to be an important problem at the stress levels needed to design for a lifetime of 20 years or longer.

Acknowledgements

References

1. F. C. Frank: *Proc. Roy. Soc. Lond. A*, 1970, **319A**, 127.
2. A. Ciferri and I. M. Ward: 'Ultra-high modulus polymers'; 1979, Barking, Applied Science.
3. M. G. Dobb, D. J. Johnson and B. P. Saville: *J. Polym. Sci.*, 1977, **58**, 237–251.
4. V. I. Kostikov: 'Fibre science and technology', 1st edn; 1995, London, Chapman & Hall.
5. M. H. Lafitte and A. R. Bunsell: *J. Mater. Sci.*, 1982, **17**, 2391–2397.
6. A. K. Rogozinsky and S. L. Bazhenov: *Polymer*, 1992, **33**, (7), 1391–1398.
7. C. J. M. Van Den Heuvel: 'Time to failure of twaron 1000 yarns'; 2000, Arnhem Twaron Products Research Institute.
8. H. H. Yang: in 'Fibre reinforcements for composite materials', (ed. A. R. Bunsell); 47; 1988, Amsterdam, Elsevier.
9. M. G. Dobb, D. J. Johnson and B. P. Saville: *Polymer*, 1981, **22**, 961.
10. M. G. Dobb, D. J. Johnson and B. P. Saville: *J. Polym. Sci.*, 1977, **15**, 12, 2201–2211.
11. R. E. Wilfong and Zimmerman: *J. Appl. Polym. Sci.*, 1977, **31**, 1–21.
12. H. H. Yang: 'Kevlar aramid fibre', 19; 1992, New York, John Wiley & Sons.
13. K. H. Gardner, A. D. English and V. T. Forsyth: *Macromolecules*, 2004, **37**, 9654–9656.
14. M. G. Northolt and J. J. van Aartsen: *J. Polym. Sci.*, 1973, **11**, 333.
15. B. Dalmolen: Proc. 3rd MERL Conf. on 'Oilfield engineering with polymers', London, UK, October 2001, MERL, 249–254.
16. 'Reinforced thermoplastic pipe for the transport of gaseous fluids', ISO TS 18226, 2005.
17. 'Implementation of reinforced thermoplastic pipe (RTP) in the oil and gas industry', RTP JIP Final Report, University of Newcastle, 2006.
18. 'Guideline for the application of reinforced thermoplastic pipe (RTP) in the oil and gas industry', RTP JIP documentation, University of Newcastle upon Tyne, Newcastle Upon Tyne, UK, 2005.
19. American Petroleum Institute: 'Recommended practice for qualification of spoolable reinforced plastic line pipe', API 15S, August 2005.
20. 'Standard test method for obtaining hydrostatic design basis for thermoplastic pipe materials', ASTM-D 2837-98a.
21. 'Thermoplastic pipes for the transport of fluids – methods of extrapolation of hydrostatic stress rupture data to determine the long-term hydrostatic strength of thermoplastic pipe materials', ISO 9080, 2003.
22. H. Eyring: *J. Chem. Phys.*, 1936, **4**, 283–291.
23. M. G. Northolt: *Eur. Polym. J.*, 1974, **10**, 799.